Computer Communications 153 (2020) 196–207

Contents lists available at ScienceDirect

Computer Communications

journal homepage: www.elsevier.com/locate/comcom

# Cascading handcrafted features and Convolutional Neural Network for IoT-enabled brain tumor segmentation

Hikmat Khan [a,1], Pir Masoom Shah [a,1], Munam Ali Shah [a], Saif ul Islam [b,*], Joel J.P.C. Rodrigues [c,d]

[a] Department of Computer Science, COMSATS University, Islamabad, Pakistan
[b] Department of Computer Science, KICSIT, Institute of Space Technology, Islamabad, Pakistan
[c] Federal University of Piauí (UFPI), Teresina - PI, Brazil
[d] Instituto de Telecomunicações, Portugal

ARTICLE INFO

*Keywords:*
IoT
Gliomas
Glioblastoma
Brain tumor
Segmentation
Deep learning
Convolutional neural network
SVM
Handcrafted features

ABSTRACT

The Internet of Things (IoT) has revolutionized the medical world by facilitating data acquisition using various IoT devices. These devices generate the data in multiple forms including text, images, and videos. Given this, the extraction of accurate and useful information from the massive serge IoT generated data is a highly challenging task. Recently, the brain tumor segmentation from IoT generated images has emerged as a promising issue that requires sophisticated and efficient techniques. The accurate brain tumor segmentation is challenging due to large variations in tumor appearance. Existing methods either use handcrafted features based techniques or Convolutional Neural Network (CNN). In this paper, a novel cascading approach for fully automatic brain tumor segmentation has been proposed, which intelligently combines handcrafted features and CNN. First, three handcrafted features are computed namely mean intensity, Local Binary Pattern (LBP) and Histogram of Oriented Gradients (HOG) and then Support Vector Machine (SVM) is employed to perform pixel classification that results in Confidence Surface Modality (CSM). This CSM along with the given Magnetic Resonance Imaging (MRI) is fed to a novel three pathways CNN architecture. In the experiments on BRATS 2015 dataset, the proposed method achieves promising results with Dice similarity scores of 0.81, 0.76 and 0.73 on complete, core and enhancing tumor, respectively.

## 1. Introduction

The emergence of IoT has enabled varied digital applications including smart health [1,2], smart homes [3], smart cities [4,5], smart buildings [6] and smart transportation system [7] to enact the Ambient Assisted Living (AAL). In this context, the smart health has been amongst the highest priorities throughout the history of human life. The applications of IoT in medical field have introduced numerous opportunities to design and develop highly sophisticated applications to solve several complicated human health issues [8]. However, it has also created many complexities in terms of acquiring, pre-processing, processing, extracting and presenting the accurate and meaningful information from generated data. Hence, the intelligent and adaptive techniques are required to extract the desired data in comprehensive form from a huge volume of data. In multiple Internet of Medical Things (IoMT) applications, the generated data is in the form of images where each image has a number of pixels and requires the efficient, automatic and advanced segmentation techniques.

Brain tumor is one of the mental health diseases that results in psychiatric symptoms (i.e., depression, anxiety disorders, panic attacks, personality change, abulia, auditory and visual hallucinations, mania, or memory difficulties), ultimately, degrades the quality of life. Early diagnosis of brain tumor plays an important role such as it increases the possibilities of the successful treatment [9,10]. Moreover, the survival chance of patients with a tumor is also increased if this mental disease is detected at early stages. Gliomas are the most common primary brain tumor with highest mortality rate and prevalence [11]. In the United States (US) alone, 80,000 new cases of primary brain tumor are expected to be diagnosed in 2020. It can be graded as either High Grade Gliomas (HGG) or Low Grade Gliomas (LGG) [12]. The HGG is infiltrated and more aggressive in nature while LGG is less aggressive in nature [12].

Accurate brain tumor segmentation has a great impact on improvement of brain tumor diagnosis and follow-up evaluations. However, it is usually performed manually which is time-consuming, extremely laborious and subjected to inter- and intra-errors which are difficult to characterize. Thus, accurate fully automated or semi-automated methods for gliomas segmentation are required [13]. Further, it is a stiff challenge because brain tumor is often pictured diffused or poorly

* Corresponding author.
*E-mail address:* saiflu2004@gmail.com (S. ul Islam).
[1] H. Khan and P.M. Shah have equally contributed in this research.

https://doi.org/10.1016/j.comcom.2020.01.013
Received 30 September 2019; Received in revised form 19 December 2019; Accepted 5 January 2020
Available online 16 January 2020

contrasted and it appears in tentacle-like structure in MRI images. Another fundamental difficulty with brain tumor segmentation is that the tumor can appear in any kind of shape, could have variable sizes and fuzzy boundaries. In addition, the exact location of such abnormalities is highly dynamic. The MRI images may also present significant challenges depending on the type of MRI images, acquisition protocol such as intensity inhomogeneity [14] and lack of standard and quantifiable interpretation of image intensities [15]. As a consequence, the grayscale values of various identical cells can be pictured highly dissimilar at different hospitals.

To overcome these challenges, more than one MRI modalities are employed e.g. T1 (spin-lattice relaxation), T1-contrasted (T1C), T2 (spin-spin relaxation) and Fluid Attenuation Inversion Recovery (FLAIR). These four MRI modalities assign a unique contrast-difference signature to healthy and tumorous tissue types.

Brain tumor can be divided into three different tissue regions, namely active tumorous tissues (i.e. enhancing tumor and non-enhancing tumor), necrotic tissues and edema (i.e. swelling near the tumor). Different biomedical image researchers proposed fully-automated or semi-automated brain tumor segmentation techniques based on either handcrafted features (i.e. classical Machine Learning (ML)) based techniques or data driven techniques (e.g. CNN). The handcrafted features based technique follows conventional ML pipelines (i.e. preprocessing, feature extraction and classifier training) [16–18]. Furthermore, selection of handcrafted properties or engineered features are important to model brain tumor's characteristics and to facilitate the brain segmentation while utilizing classical ML techniques.

A variety of handcrafted features are proposed in the literature: gradients [19], brain symmetry [19–21], HOG [22], LBP [23] and physical properties [21]. Moreover, various classical ML techniques using handcrafted features have been employed for brain tumor segmentation namely Neural Network (NN) [24], SVM [25,26], Adaboost [27], and Random Forest (RF) [28]. The MICCAI online BRATS challenge of 2012, 2013 and 2014 suggested the methods that rely on RF are among the most accurate methods [13,29,16,17].

Recently, different biomedical researchers used CNN based techniques for brain tumor segmentation task and achieved promising results. Urban et al. [30] proposed 3D-CNN with 3D convolutional filters, Yi et al. [31] proposed 3D-CNN with Difference of Gaussian (DoG) 3D kernels, Zikic et al. [32] applied 2D patches based 2D-CNN, Pereira et al. [33] proposed 2D patches with deeper 2D-CNN, Havaie et al. [34] proposed a two pathway 2D-CNN with global and local 2D patches.

To summarize, our contributions are as follows. First, a novel hybrid technique (combining traditional ML hand engineered features based technique i.e. SVM and CNN in cascaded manner) for brain tumor segmentation has been proposed. Since handcrafted features attempt to model the domain knowledge and CNN based approaches mainly try to generate features in unsupervised fashion, therefore, combining these distinct approaches in a cascaded manner potentially outperforms either technique based on handcrafted features or data-driven (e.g. CNN) individually. Second, we addressed the brain tumor's dynamic manifestation challenge by introducing domain inspired prior knowledge in the form of features (i.e. HOG, LBP and MI) that encode the tumor structural infromation. Moreover, we addressed the challenge of the dynamic appearance of a tumor in the brain by providing SVM's (i.e. trained on handcrafted such as HOG, LBP, and MI) generated CSM as prior knowledge to the CNN, that helped the CNN to perform fine-grained tumor shape segmentation. Besides the four MRI modalities, the CSM modality provides aditional information to CNN on tumor stucture and spatial location. To generate CSM model, three handcrafted features i.e. HOG, LBP and MI are calculated in a spatial neighborhood of size ($7 \times 7$). The selection of these three handcrafted features are inspired by domain knowledge and observations of tumor pictured in different MRI modalities. These three handcrafted features are concatenated and SVM is employed as discriminative pixel classifier. The trained SVM performs the pixel level classification into tumor or non-tumor class to generate the CSM which contains the binary values (i.e. 0 or 1 where 0 presents non-tumor and 1 presents tumor). Third, we proposed Three Pathways CNN (TP-CNN) architecture comprised of three parallel pathways — Confidence Surface Global Pathway (CSGP), MRI Local Pathway (MRILP) and MRI Global Pathway (MRIGP). The CSGP is shallow in depth with fewer stacked convolutional layers that takes CSM as input and generates intermediate feature maps. The MRIGP and MRILP process original MRI modalities in shallow and deeper pathways (i.e. layers), respectively, and generate feature maps of same dimensions as CSGP. The output of three pathways are combined by concatenating their respective feature maps into TP-CNN. The concatenated feature maps are followed by one convolutional layer, two fully connected layers and the softmax classifier that perform the final center pixel-level classification. The cascaded combination of handcrafted based technique and data driven CNN has not only enabled us to leverage the maximum out of both distinct techniques and simultaneously introduced domain expertise for consideration but also to obtain comparable results to the recent state-of-the-art methods.

Rest of this paper is organized as follows. Section 2 investigates the relevant existing research. Section 3 provides the details of the proposed model. Section 4 describes the dataset and experimental setup details. Section 5 presents the evaluation of the proposed technique. Finally, Section 6 presents the concluding remarks and future work.

## 2. Related work

In last few decades, an exponential increase in the research related to brain tumor segmentation has been observed [13,18]. The findings of these works highlight the importance of automation in brain tumor segmentation. Moreover, they also stress on the needs to propose and implement novel algorithms to cope with the issues and challenges faced in this domain.

Majorly, the brain tumor segmentation can be categorized in two types of models — generative and discriminative models. The techniques based on the generative models, heavily relies on the domain specific previous information on the appearance, location and volume of healthy tissues [35–38]. Prastawa et al. [39] use the International Consortium for Brain Mapping (ICBM) atlas that provides robust estimates of probabilities for healthy brain structure, spatial location and dispersion of different healthy brain tissues (i.e. WM, GM, and CSF). These prior probabilities or estimates on the tumors structure and spatial locations are treated as expert prior knowledge and used to extract the unknown tumor regions. The ICBM atlas aligns with brain to compute posterior probabilities of the WM, GM and CSF. The deviation from healthy brain tissues are noted with lower posterior probabilities and detected as abnormalities. Iqbal et al. in [40] employed three different architectures namely SENeT, Interpolated Network (IntNet) and Skip-net for brain tumor segmentation. Their claimed means results for three networks are presented in Table 1. In [41], the authors proposed an end-to-end network named residual cyclic unpaired encoder–decoder network (RescueNet). Similarly, Muhammad et al. [42] proposed, a novel deep learning based multigrade brain tumor classification system. They used data augment to increase the training dataset. The result of their fine-tuned VGG-19 can be seen in a detailed Table 1.

Schmidt et al. [43] computed four Alignment Based (AB) properties at multi-scales — spatial binary mask, spatial likelihood of normal tissues, average intensities and left to right brain symmetry. The AB features encoded spatial anatomic information then combined to trained soft margin SVM to discriminate tumor from normal regions. They aslo incorporated the textural features with AB features on multiple scales that further aided in discrimination of the tumor region from normal regions. Gering et al. [44] proposed a framework that was trained exclusively on normal healthy tissue. They attempt to recognize the deviation from the normalcy in order to compute the fitness map. Such approaches are used to fix the irregular structures.

Other researchers proposed knowledge based system and follow a coarse to define strategy for brain tumor segmentation. In this regards, Agn et al. [45] presented a fully automated generative method that modeled the brain tissues with Gaussian Mixture Models (GMM) combined with atlas priors of healthy tissues. Their extended version also modeled the tumor shape using Convolutional Restricted Boltzmann Machines (CRBM) in order to generate prior on tumor manifestation and spatial extents. The atlas base probabilistic model incorporated the additional spatial prior on tumor shape and performed healthy tissues segmentation. The experimental results showed that generative methods employing tumor prior performed well particularly on whole tumor region segmentation, hence, justify the significance of providing the additional prior on the shape of tumor. The typical generative models for brain tumor segmentation using MRIs are given in [39,43,44,35,45].

Discriminative models have also been applied for brain tumor segmentation. Contrary to generative models, discriminative models rely on the extraction of low level handcrafted features, which directly models the relationship between the input image and ground truth. In discriminative models, selection criteria for highly discriminative and pertinent features are heavily influenced by the domain or expert knowledge. The quality of the segmentation is highly dependent on the relevancy of handcrafted features and chosen ML technique. The more appropriate they are; the better quality of segmentation will be obtained. In this regards, different approaches used different handcrafted features with various classical ML technique for brain tumor segmentation. For instance, Hamamci et al. [46] used the raw pixel intensities as discriminative features, Tustison et al. [21,47] employ supervised brain tumor segmentation framework based on multi-modality intensity, geometry and asymmetry and symmetry related features, Subbanna et al. [48] applied Gabor filter, Kadi et al. [49] proposed textural fractal characteristics, Baur et al. [50] used local image texture and edge features, Zacharaki et al. [51] applied tumor shape, intensity characteristics and rotation invariant texture features, Subbanna et al. [52] utilized texture features such as Gabor filter banks, Islam et al. [27] used multi-fractal Brownian motion features, Bauer et al. [25] proposed multispectral intensities and texture features and Reddy et al. [53] computed the HOG, LBP and MI in pixel spatial neighborhood. Various discriminative classifiers using handcrafted features have been employed for brain tumor segmentation [13,29,16,17].

Recently, deep learning has evolved as a powerful technique in comparison to ML approaches and achieved state-of-the-art results on variety of computer vision and biomedical imaging tasks [54,50,55]. In particular, CNN achieves promising results on different online competitions and challenges of image classification [56–58], video classification [59], object recognition [60,61] and biomedical image segmentation [13,62]. Deep learning techniques have the capability to learn highly discriminative features in increasingly complex hierarchy directly from in-domain data. Due to this dynamic features learning capability, deep learning based methods often outperform handcrafted feature based methods. In this context, Bhanumathi et al. [62] used CNN models to fine tune the brain tumor images. Similarly, Urban et al. [30] proposed multi-modal 3D-CNN with 3D spatial convolutions for glioma segmentation task. In this regards, 3D patches of MRI are fed to CNN to perform the prediction of the center voxel. Yi et al. [31] developed a unique 3D-CNN framework to decouple the image pixels. The 3D-CNN defined a convolutional layer with pre-defined Difference of Gaussians (DoG) filters to perform true 3D convolution incorporating local spatial neighborhood information at each pixel. Kayalibay et al. [63] demonstrated the 3D-CNN based medical image segmentation model on hand and brain MRI, which combine the multiple segmentation maps created at different scales. Moreover, different biomedical image researchers proposed 3D-CNN model for biological image segmentation [18,50].

Medical image segmentation includes various issues that are required to be addressed, for instance, high class imbalance, scarcity of data, and high memory requirements of 3D images. Moreover, fully 3D-CNN comes with increased number of parameters that demand high medical data during training, slow inference and significant memory and computational requirements. As a result of these observations, it is always discouraged to use 3D-CNN especially in the field of medical for segmentation tasks. Zikic et al. [28] addressed these challenges and proposed standard 2D-CNN architecture based on 2D patches that were extracted from 2D slices of MRI modalities. Their method achieved comparable results and reduced computational cost simultaneously. Recently, Hussain et al. [64] introduced five different CNN based approaches for glioma tumors segmentation which are evaluated on BRATS 2013 and 2014 datasets. Pereira et al. [33] further evaluated the standard 2D-CNN and improved the quality of the glioma segmentation by introducing deeper 2D-CNN architectures by fixing convolutional kernel to (3 × 3) size throughout the network. With smaller size convolutional kernels, more convolutional layers are stacked. Furthermore, deeper 2D-CNN made it feasible to apply more non-linearities, which resulted the model that is less prone to overfitting, because smaller kernels have fewer weights than larger kernels [65]. Havaei et al. [66] presented two pathways 2D-CNN architectures in cascaded fashion that differs from those traditionally used in computer vision. In their proposed 2D-CNN architecture, two pathways of 2D-CNN are local and global that processed smaller and larger sized 2D patches respectively. The two different size 2D patches centered at the same spatial location, enabled their model to consider the smaller as well as the larger contextual information simultaneously, while classifying the label of the center pixel. In this line of 2D-CNN models, several novel 2D patches based CNN architectures are proposed, some of the examples are presented in [18,50]. However, the performance of these 2D-CNN models are significantly well but the quality of segmentation can further be improved by providing additional domain inspired prior knowledge about the shape, boundaries and spatial location of the tumor within the brain. In this research work, we introduce prior on the tumor shape in the form of CSM and provide it as additional input to CNN. The CSM acts as an additional source of knowledge on tumor structure, shape and spatial location that further guide our proposed method to perfom fine-grained brain tumor segmentation.

## 3. Proposed technique

We divide our framework into two phases — CSM generation and brain tumor segmentation using CNN as shown in Fig. 1. First phase is further sub-divided into six steps: MRI fusion, pre-processing, feature selection, feature extraction, feature labeling and classifier training. Section 3.1 presents the detailed discussion of each step. The aim of first phase is to capture high level tumor manifestation details and generate the CSM that comprises of estimated prior knowledge on the tumor appearance and spatial location. In second phase, the CSM along with T1, T1c, T2, and Flair MRI modalities are fed to three pathways CNN in order to perform accurate brain tumor segmentation. Section 3.4 contains the detailed discussion on each step of second phase.

### 3.1. Confidence surface modality (CSM) generation

#### 3.1.1. MRI fusion and pre-processing

The pixel wise intensities addition of T1, T1c, T2 and FLAIR MRI result in fused MRI modality as shown in Fig. 2. The fused MRI modality gathers pixel level information across T1, T1c, T2 and FLAIR in a single modality (i.e. fused MRI). The MRI acquisition itself introduces challenges, like same tissues obtain different intensity signature within the same MRI image. In order to address these challenges, we used bias field correction technique i.e. N4ITK [14]. However, bias field correction alone is not enough, hence, we also employed intensity normalization technique proposed by Nyul et al. [15]. It is important to make sure that similar tissues take similar intensity distribution not only within the same MRI slice but across all the MRI slices.

**Table 1**
Summary of literature review results.

| Author | Method | Dataset | WholeTumor | CoreTumor | ActiveTumor | Accuracy | Year |
|---|---|---|---|---|---|---|---|
| Urban et al. | 3D-CNN model applying 3D convolutional filters | BRATS2015 | 0.87 | 0.77 | 0.73 | – | 2014 |
| Zikic et al. | 2D patches are extracted slice wise employed with 2D-CNN | BRATS2015 | 0.83 | 0.73 | 0.69 | – | 2014 |
| Havaei et al. | Local and global 2D patches with cascaded two path ways 2D-CNNs | BRATS2015 | 0.88 | 0.79 | 0.73 | – | 2016 |
| Pereira et al. | 2D patches are extracted slicewise with deeper 2D-CNN with fixed convolutional filter 3 × 3 | BRATS2013 | 0.88 | 0.83 | 0.77 | – | 2016 |
| Pereira et al. | 2D patches are extracted slicewise with deeper 2D-CNN with fixed convolutional filter 3 × 3 | BRATS2015 | 0.78 | 0.83 | 0.75 | – | 2016 |
| Davy et al. | Two path ways 2D-CNN for simultaneous local and global 2D patch processing | BRATS2015 | 0.83 | 0.75 | 0.68 | – | 2015 |
| Rao et al. | Extract multi2D patches around each pixel then train different layer of CNN. The output of the last hidden layers are concatenated to generate feature map for random forest as classifier. | BRATS2015 | 0.67 | – | – | – | 2015 |
| Kayahbay et al. | Extract 3D patches for 3D-CNN | BRATS2013 | 0.87 | 0.74 | 0.71 | – | 2017 |
| Kayahbay et al. | Extract 3D patches for 3D-CNN | BRATS2015 | 0.85 | 0.72 | 0.61 | – | 2017 |
| Yi et al. | 3D-CNN with difference of Gaussian kernel (DoG) | BRATS2013 | 0.89 | 0.78 | 0.71 | – | 2016 |
| Yi et al. | 3D-CNN with difference of Gaussian kernel (DoG) | BRATS2015 | 0.89 | 0.76 | 0.80 | – | 2016 |
| Iqbal et al. | SE-Net | BRATS 2015 | 0.88 | 0.81 | 0.81 | – | 2018 |
| Iqbal et al. | Interpolated Network (Int-Net) | BRATS 2015 | 0.90 | 0.87 | 0.80 | – | 2018 |
| Iqbal et al. | SkipNet | BRATS 2015 | 0.87 | 0.86 | 0.79 | | 2018 |
| Sajjad, Muhammad, et al. | VGG-19 | Radiopaedia | – | – | – | 94.58 | 2019 |
| Nema, Shubhangi, et al. | RescueNet | BRATS 2015 | 0.94 | 0.94 | 87 | – | 2020 |
| Nema, Shubhangi, et al. | RescueNet | BRATS 2015 | 0.94 | 0.85 | 93 | – | 2020 |

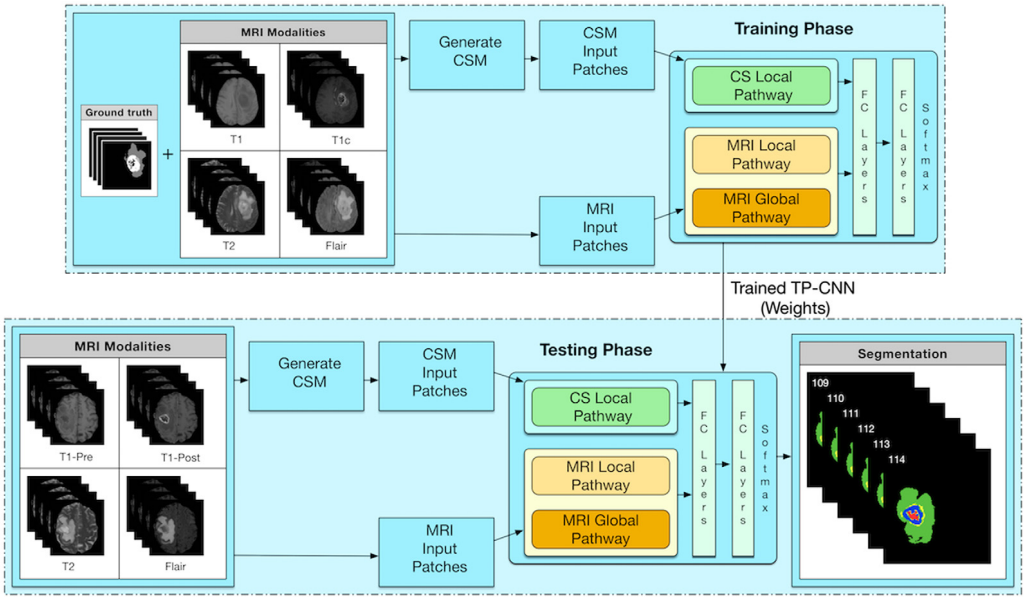


**Fig. 1.** Block diagram showing the overall framework. The upper dotted box presents work flow of the training phase of TP-CNN, whereas, the lower dotted box presents the testing phase of TP-CNN. (Better viewed in color).

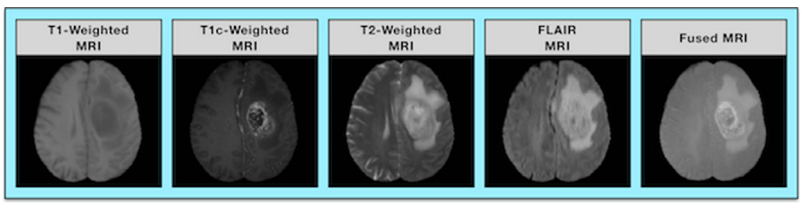


**Fig. 2.** Left to right: Four MRI modalities (i.e. T1, T1c, T2 and FLAIR) and fused MRI modality. The fused MRI modeality is pixelwise addition of T1, T1c, T2 and Flair. (Better viewed in color).

### *3.1.2. Feature selection*

The domain knowledge always plays a vital role in the selection of criteria and pertinent features, which has direct impact on quality of the solution. During the feature selection, the focus is mainly on the selection of group of most effective and relevant feature descriptors, which maximally model the expert observations. Among many possible feature descriptors, we have selected HOG, LBP and MI as feature descriptors. Since the tumor can appear in variable shape, size, poorly

contrasted, diffused intensities and fuzzy boundaries, the best suited set of feature descriptors for such challenge must have the characteristics to capture the intensity enhancement, textural and gradient information. Brain tumor pictured in MRI can be seen as sharp or abnormal transition in intensity distribution. Furthermore, these non-uniformities in intensity regions have high degree of textural variabilities and tumor often having fuzzy boundaries. Using these observations, it is concluded that the combination of HOG, LBP and MI feature descriptor can closely address such challenges. The combination of these feature descriptors has been successfully used in texture classification, human detection and face recognition [22,67,68]. The LBP feature descriptor [68], likewise, HOG descriptor [22], has also been successfully used in variety of computer vision and image processing tasks: For instance, in object detection and recognition. The HOG has the capability to encode the sharp transition of intensity gradient on tumor boundaries while LBP and MI have been used to capture the intensity variation and textural detail of tumor. The HOG is applied to detect tumor boundaries information, while LBP and MI is used to capture the detailed textural and average intensity enhancement information.

#### 3.1.3. Feature extraction

The three feature descriptors HOG, LBP and MI are computed in spatial neighborhood of ($7 \times 7$) which are then concatenated into a single feature vector that encodes intensity variation, intensity enhancement and gradient information. According to the American Brain Tumor Association (ABTA) observations, the mass of the abnormal region is significantly smaller than healthy region [69]. This means, if the features at each pixel location are computed then it will end up with a large number of negative samples than positive samples which will raise the class imbalance issue. The classifier trained with imbalance classes will overfit and result in biased classification. The imbalance class challenge has been addressed by introducing vertical, horizontal and depth strides concept within the MRI image. After performing several experiments, stride values for tumor and non-tumor regions are considered. For non-tumor region, horizontal, vertical and depth stride values are set to 3, 5 and 1, respectively, while for tumor regions, all the three stride values are set to 1. For example, only compute healthy brain feature vectors in spatial neighborhood of ($7 \times 7$) if center pixel belongs to non-tumor region and pixel spatial dimensions $x, y, z$ are divisible on horizontal, vertical and depth stride, respectively. The same is done for tumor class but as the stride size is 1 in all dimensions, feature vectors at each pixel location are computed for tumor class. Furthermore, the whole brain mask is employed that speeds up the process by computing the feature vectors within the brain region only and eliminating unnecessary feature vectors calculation for the background region (i.e. non-brain region in MRI image). In this way, both positive and negative samples have been generated in nearly equal number that not only makes brain tumor segmentation a supervised ML problem but also addresses the classes imbalance challange.

#### 3.1.4. Feature labeling and training

The MICCAI BRATS-2015 dataset provides annotated ground truth for patients. The given ground truth has been considered in order to perform class labeling of the feature vectors computed in neighborhood of ($7 \times 7$). Each computed feature vector is assigned with positive or negative class label. The feature vector has been assigned a positive class label if the pixel at the same location in ground truth is positive. Similarly, the feature vector has been assigned a negative class label if the pixel at the same location in ground truth is also negative. Together, the positive and negative feature vectors define the training dataset for SVM classifier. Then, RBF-SVM [70] has been trained as the discriminative pixel classifier. Moreover, a separate SVM for HGG and LGG datasets are trained. SVM training steps are shown in Fig. 3.

#### 3.1.5. Confidence surface modality generation

The trained SVM performs binary classification of each pixel of fused MRI that decides the pixel class i.e. whether it belongs to the tumor or non-tumor class which ultimately results in CSM. The pixel classification of SVM gives us confidence surface that consists of the pixel level information of each class (i.e. tumor or non-tumor pixel). It is called as pixel level confidence surface termed as CSM. The CSM highlights the abnormal spot in the brain as can be seen in Fig. 3. The construction of CSM can be considered as target output of the first phase, The Fig. 7 presents generated CSM and fused MRI.

### 3.2. Pre-processing

During MRI acquisition, different types of noise and intensity variations are introduced. In order to minimize the effect of such deviations on classification results, different methods are introduced, some of them are intensity normalization, bias correction such as N3ITK and N4ITK and de-noising methods [34,33]. In order to address the bias field distortion, we applied N4ITK [14] that followed by intensity normalization technique proposed by Nyul et al. [15].

### 3.3. Patches extraction

The 3D-CNN models for brain tumor segmentation accept 3D patches, basically cube of voxel, that result in increased number of model's parameters, hence demand large training dataset. In contrast, due to the 2D nature of our model, it has lesser number of parameters, hence, it does not demand large training dataset. In order to extract 2D patches from 2D MRI slices, we sampled 2D patches of size ($33 \times 33$) for each sub tumor region from different MRI modalities (i.e. T1, T1c, T2 and FLAIR) and CSM. Each patch is associated with different input modality centered at the same pixel location. Moreover, 2D patches are extracted in balance ratio for all five classes — healthy brain, core tumor, necrosis, enhancing, non-enhancing and edema that enabls us to effectively handle imbalance classes issue. The 2D patches that are extracted from T1, T1c, T2 and FLAIR modalities are processed by MRILP and MRIGP, while the 2D patches that are extracted from CSM are processed by CSGP pathway.

### 3.4. Proposed convolutional neural network approach

During the second phase of the proposed framework, we define the proposed model's architecture that accepts 2D patches extracted from original MRIs and CSM as input and performs the fine-grained brain tumor segmentation. The CSM constructed in the phase one of the proposed framework contains additional information on the tumor manifestation. It is provided as additional input to our proposed TP-CNN model. The TP-CNN architecture is further divided into three different pathways where each pathway processes different information and extracts different level of details (i.e. features). The three model's pathways are termed as Confidence Surface Global Pathway (CSGP), MRI Local Pathway (MRILP) and MRI Global Pathways (MRIGP). A separate TP-CNN architecture has been proposed for HGG and LGG datasets. The detailed diagrams of TP-CNN for HGG dataset is shown in Fig. 4. The detailed discussion on MRILP, MRIGP and CSGP is presented in Section 3.4.1.

#### Initialization

In deep neural networks, right weights initialization reduces the convergence time and bring stability to the loss function. There are various weights initialization techniques that can be used: all zero initialization, Gaussian random variable and Xavier initialization [71,72]. The all zero weight initialization technique is inappropriate since all the neurons are computing the same output and no gradient would flow on back propagation. The Gaussian random distribution of zero mean and small standard deviation [71] initialization is only suitable

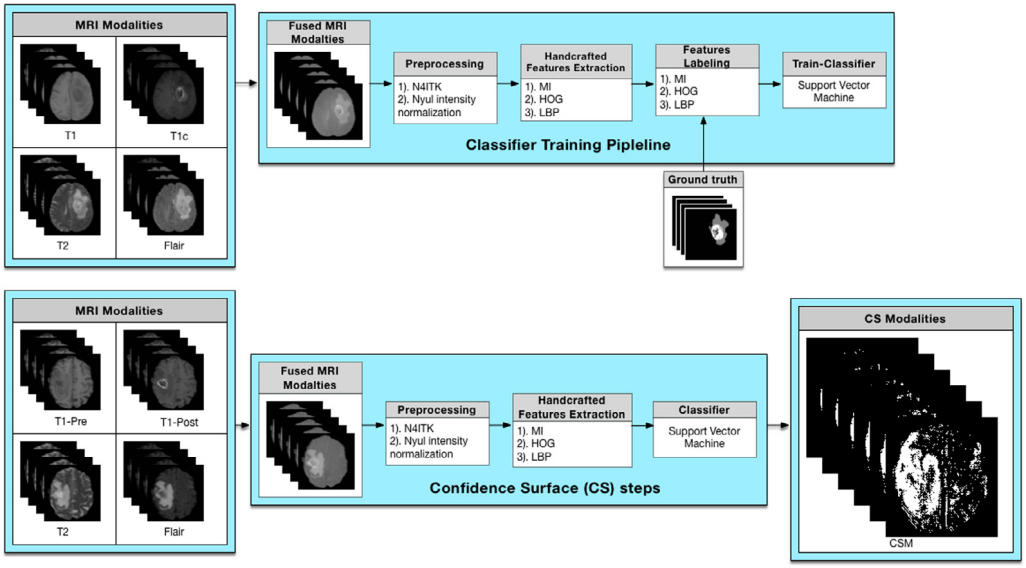


**Fig. 3.** Top to bottom: Upper figure presents the SVM training pipeline for CSM generation. At first step, T1, T1c, T2 and FLAIR are fused to generate fused MRI. At second step, intensity normalization over fused MRI has been performed. At third step, feature extraction has been applied, then the extracted feature vectors are labeled. Finally, the labeled feature vectors are used for training SVM. Lower figure presents CSM generation pipeline. Initially, MRI modalities are fused and intensity normalization is performed on fused modality. Further, feature vectors (i.e MI, LBP and HOG) are extracted at each pixel location in a spatial neighborhood of (7 × 7). Finally, each CSM's pixel is assigned the SVM predicted class label. (Better viewed in color).

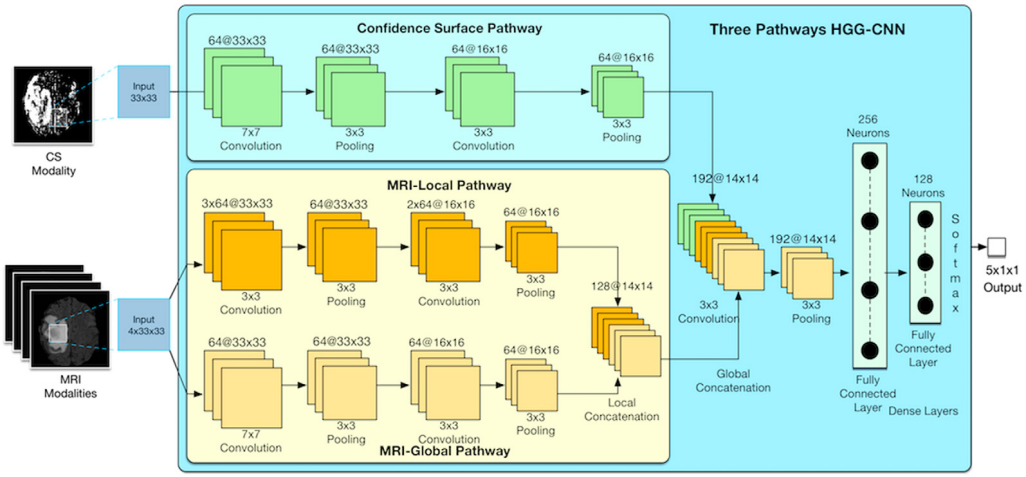


**Fig. 4.** TP-CNN architecture for HGG dataset where each block represents the fundamental operation of CNN (i.e. Convolution, Max-Pooling, Feature Maps, FC Layers, and Softmax). (Better viewed in color).

for shallow network because of very small gradients. In order to make the convergence reliable many researchers suggested to use the Xavier initialization [72]. In Xavier initialization, gradients are maintained in controlled manner and the risk of gradient explosion or vanishing is reduced.

$$Var(w) = \frac{2}{n_{in} + n_{out}} \tag{1}$$

In Eq. (1), $n_{in}$ shows the fed in while $n_{out}$ presents the fed out neurons, respectively.

*Activation function*

Activation functions introduce the non-linearity into the system. There are many activation functions proposed in literature and it is still an active research area. Some of the most commonly used activation functions are sigmoid, hyperbolic tangent, Rectified Linear Unit (ReLU), Leaky Rectified Linear Unit (LeakyReLU) and parametric ReLU [73, 56,60]. LeakyReLU is the advanced version of ReLU that handles the dying ReLU problem by introducing the negative gradients [73]. We used LeakyReLU as the activation function. Below equation presents the mathematical form of LeakyReLU.

$$f'(x) = f(x) + \alpha \ \min(0, b) \tag{2}$$

In Eq. (2), x presents input, b is negative slope coefficient while $\alpha$ is leakiness and it value varies between 0 and 1.

*Pooling layers*

Pooling is used to reduce the dimensionality of the feature maps. It makes the model invariant to small intensity, whereas, illumination changes are not significant and should be ignored. The most commonly used pooling is max pooling, average pooling [74]. We used Max pooling that selects the features with maximum value in pooling kernel. The pooling kernel size and stride determine the dimensions of the output feature maps. For example, consider the feature map with dimension of (32 × 32) and pooling is used with kernel size of (4 × 4) and stride of 2, the dimensions of the output feature map will be (14 × 14). It can

be formalized as follows:

$$pool_{i,j} = \max_{p} f(x)_{i+p,j+p} \tag{3}$$

In Eq. (3), $i$ and $j$ are the spatial positions.

*Regularization*

The regularization prevents the network from overfitting. There are several regularization schemes available. L1 and L2 are most commonly used regularization techniques. Another effective, simple and recently introduced regularization technique is Dropout [75]. During training step, Dropout regularizer randomly switches on and off the neurons and forces each neuron to learn and contribute independently to overall output of the network. We used Dropout as the regularizer in fully connected layers. It can be formalized as follows:

$$y_i = \sum_{N \ \epsilon \ N^*} Pr(n) y_i^N \tag{4}$$

In Eq. (4), where $y_i$ is the expected output of the unit, $i$ and $N^*$ are the set of all small networks created with dropout, $y^N$ is the output of unit $N$ where $Pr(n)$ is the probability of the small network.

*Fully connected layers*

At the end of the convolution operations, network normally has a fully connected layers, where each pixel of the feature map is considered as neuron that is forwarded to fully connected layers. We introduced two fully connected layers in both HGG and LGG TP-CNN architectures. For HGG TP-CNN, first layer comprised of 256 while the second layer has 128 neurons, whereas, LGGTP-CNN first layer consists of 512 and second layer consists of 256 neurons. The softmax has been used as a classifier that performs pixel level classification. The softmax predicts each pixel as healthy tissues, necrosis, edema, non-enhancing tumor or enhancing tumor and are labeled as 0, 1, 2, 3, and 4 respectively. The Eq. (5) presents formalized form of softmax using Bayes Theorem [76].

$$p(C_t|x) = \frac{p(x|C_t)\ p(C_t)}{\sum_{j=1}^{n} p(x|C_j)\ p(C_j)} \tag{5}$$

In Eq. (5), $C_t$ represents the probability of the selected class while $C_j$ is the probability of the remaining classes for $j = \{1, 2, 3, \ldots, nth\}$ where $C_j$ is not equal to $C_t$. It can be written in exponential form [76].

$$\sigma(a)_k = \frac{e^{a_k}}{\sum_{j=1}^{n} a_j} \tag{6}$$

*Loss function*

The loss function measures the compatibility between predicted and given ground truth label. We used the categorical cross-entropy as loss function.

$$Loss = -\sum_{j \ \epsilon \ voxels} \ \sum_{k \ \epsilon \ classes} c_{j,k} \ \log(\hat{c}_{j,k}) \tag{7}$$

In Eq. (7), c is the true target class whereas $\hat{c}$ is the predicted class

*3.4.1. Three pathways CNN (TP-CNN) architecture*

The proposed TP-CNN has three pathways. Each pathways is dedicated to process 2D patches extracted from respective (i.e. either CSM or MRI) modality. For instance: CSGP is dedicated to process 2D patches of $(33 \times 33)$ extracted from CSM whereas MRIGP and MRILP are designed to process the 2D patches that are extracted from T1, T1c, T2 and FLAIR, with different number of stacked convolutional layers. The deeper MRILP pathways with smaller kernel size allow us to stack more convolutional layers with more non-linearities applied and fewer weights that make the CNN less prone to overfitting [65] whereas, both MRIGP and CSGP are equal depth and shallow pathways as compared to MRIGP. The shallow depth enables them to learn the high level features from 2D patches. Finally, the feature maps of all three pathways are combined. It is important to mention here that feature maps of CSGP act as additional source of knowledge that are extracted from CSM. Moreover, as mentioned in Section 3, there are more patients for HGG than LGG that causes an imbalance classes issue. These observations motivate us to propose a separate TP-CNN architecture for HGG and LGG. The HGG TP-CNN stacks more convolutional layers (i.e. deeper) and non-linearities than LGG TP-CNN (i.e. shollow). The Figs. 4 and 5 present the overall architectures of the proposed HGG and LGG TP-CNN models, respectively.

### 3.5. Classification, segmentation and post processing

Tumor region can be divided into four different sub-regions — enhancing tumor, non-enhancing tumor, necrosis and edema (i.e. swelling around or near the tumor). The goal of the brain tumor segmentation method is to locate and segment out the tumorous region. According to literature review, researchers segment out the tumor into three regions — whole tumor (all tumor regions), core tumor (all tumor components except edema) and enhancing tumor (only active tumor region). The brain tumor classification task has been approached as multi-class classification problem. Each pixel is classified in one out of five classes i.e. either healthy brain (i.e. non-tumor), edema, necrosis, enhancing and non-enhancing tumor. The T1, T1c, T2 and FLAIR modalities along with CSM are converted to 2D slices then 2D patches of size (33×33) are extracted with stride of $(1 \times 1)$ horizontally. The extracted 2D patches are fed to model to assign label (i.e. model pixel classificaiton) to each pixel location. After the pixel classification, we color each predicted pixel location according to our defined coloring scheme. Our coloring scheme for intra-tumoral classes is — green color is used for edema, red is used for necrosis, yellow is used for enhancing and blue is used for non-enhancing tumor. As for post-processing, a simple 8-neighbors connected algorithm is applied that returns the flat blobs with highest connected components [77]. The end-to-end workflow of our proposed system can be seen in Fig. 6.

## 4. Experimental setup

### 4.1. Dataset and implementation details

The MICCAI BRATS-2015 dataset has been used in order to evaluate our model. The MICCAI BRATS dataset is considered a benchmark dataset for brain tumor segmentation. It not only provides real world patients data but also gives a ground truth for training data that is annotated by professional neurologists. For implementation, scikit-learn [78], Keras libraries [79] and SimpleITK [80] are used.

### 4.2. Training

The hyper-parameters that are used to train HGG and LGG TP-CNN are presented in Table 2. For training, $500,000$ patches of size $(33 \times 33)$ for HGG and 400,000 patches of same size are extracted for LGG TP-CNN architectures. The 10-fold cross validation is applied in order to assess the validity of our model. Moreover, the data augmentation technique has been adopted for both HGG and LGG. In order to augment the data, we rotate each patch by multiple of 90 degree (i.e. 90,180 and 270 degree). Such data augmentation technique helps not only in increasing the amount of training data four times but also prevent the models from overfitting.

## 5. Results and discussion

We used Dice Similarity Score (DSS) to quantify the segmentation accuracy of our proposed method on BRATS-2015 dataset. The DSS measures the similarity between given ground truth and predicted result. It is the most commonly used performance measure to evaluate brain tumor segmentation results [18]. The mathematical formulation of DSS is given in Eq. (8). In Eq. (8), $P_1$ presents the segmented or

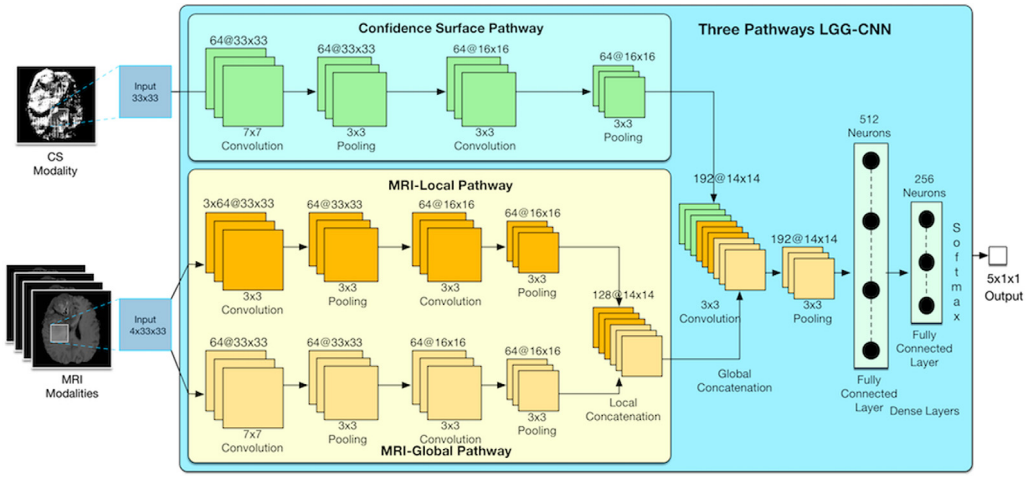


**Fig. 5.** Presents TP-CNN architecture for LGG dataset where each block presents the fundamental operations of CNN (i.e. Convolution, Max-Pooling, Feature Maps, FC Layers, and Softmax). (Better viewed in color).

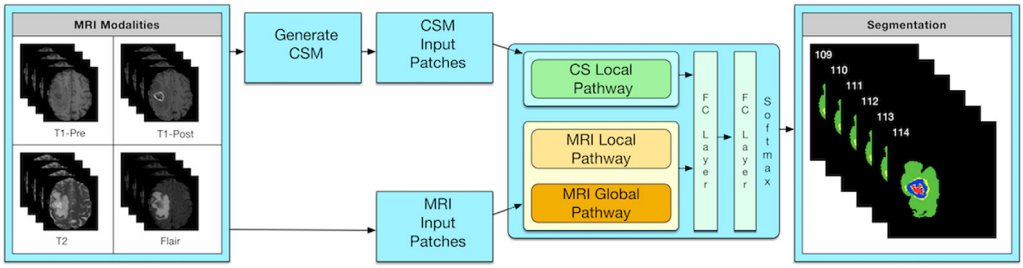


**Fig. 6.** Presents the end-to-end workflow of our framework in a block diagram, for instance, from input modalities T1, T1c, T2 and FLAIR to final output segmentation result. The CS local pathway processes the CSM 2D patches. The MRI local and MRI global process the 2D patches sampled from original MRI modalities. The FC stands for fully connected layer, CSM stands for SVM predicted CSM. (Better viewed in color).

**Table 2**
Training phase hyper-parameters for TP-CNN.

| Parameter | Values for HGG | Values for LGG |
|---|---|---|
| Initial Weights | Xavier normal initializer | Xavier normal initializer |
| Leaky ReLU ($\alpha$) | 0.333 | 0.333 |
| Momentum ($\upsilon$) | 0.9 | 0.9 |
| Nesterov's accelerated momentum | True | True |
| Learning Rate ($\eta$) | 0.003 | 0.003 |
| Decay | 0.001 | 0.0001 |
| Dropout | 0.1 | 0.5 |
| Batch Size | 128 | 128 |
| Epochs | 20 | 25 |

predicted tumor region by proposed method, $T_1$ represents the manual segmentation (i.e. given ground truth). The symbol ($\wedge$) shows the pixel wise logical AND operation, and ($|.|$) presents the set cardinality.

$$Dice = \frac{2|P_1 \wedge T_1|}{|P_1| + |T_1|} \tag{8}$$

Fig. 7 shows CSM generated using the proposed technique. The label in top left shows the type of modality while the label in the bottom right shows the corresponding slice number. First row shows selected slices of fused MRI modality while the second row presents the respective CSM slice. It can be seen that CSM contains useful prior on the tumor shape. Such two step approach enables TP-CNN to achieve promising results on the whole tumor.

Following coloring scheme has been considered to represent different tumor types — green presents edema, blue shows non-enhancing tumor, red expresses necrosis and yellow means enhancing tumor. Fig. 8 presents the segmentation results of TP-CNN for HGG and LGG datasets. It can be noticed that the proposed TP-CNN leverages usefulness of prior on tumor shape and obtains fine segmentation results on the whole tumor boundaries (i.e. especially on edema). Figs. 9 and 10 show the slice wise results of HGG TP-CNN and LGG TP-CNN respectively. It can be seen from the HGG and LGG TP-CNN slice wise segmentation results, providing prior on the whole tumor shape showing their worth and enables us to eliminate the irrelevant pixels at first step from further consideration in the second step (i.e. final tumor segmentation step).

Table 3 shows results of the proposed scheme for different tumor types. The proposed TP-CNN exploited the CSM and novel three pathways architectures and obtained 0.81, 0.76 and 0.73 on complete tumor, core tumor and enhancing tumor, respectively. Our proposed technique obtained better results for segmenting whole tumor boundaries (especially, a DSS of 0.91 is obtained on edema) as compared to the intra-tumor regions. Since, CSGP of TP-CNN provides information on two classes only (i.e. either tumor or non-tumor) and does not provide information on sub-tumor regions individually. Consequently, our model did not perform that well on intra-tumor regions' segmentation. These relatively lower segmentation results on tumor sub-regions are not surprising as it is provided prior on the whole tumor shape instead of individual sub-tumor regions.

Table 4 presents the comparison of our proposed method's obtained DSS with other 2D-CNN and ML based state-of-the-art methods for brain tumor segmentation. These methods also used BRATS-2015 dataset to evaluate the performance of their proposed methods. As shown in Table 4, our proposed method has obtained promising results compared to other state-of-the-art methods.

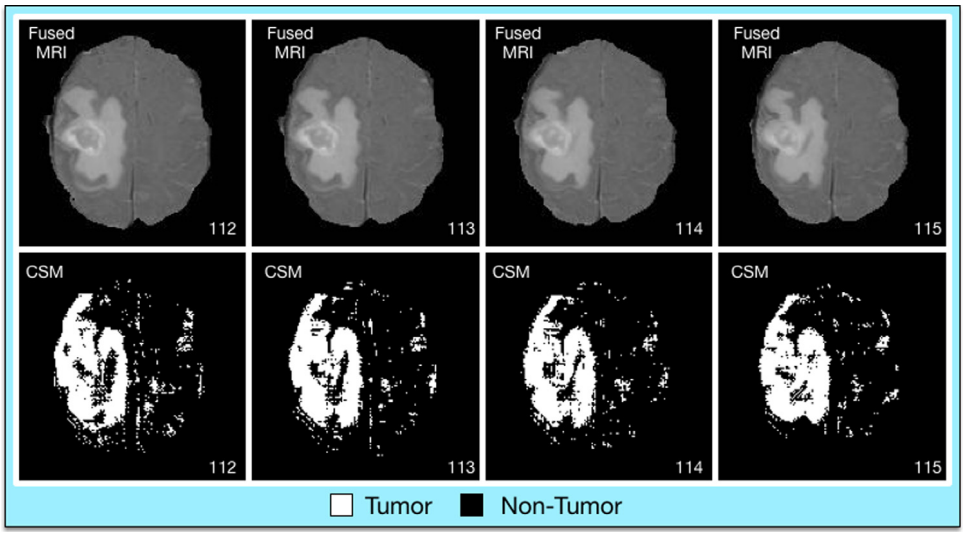


**Fig. 7.** CSM Generated by proposed technique. (Better viewed in color).

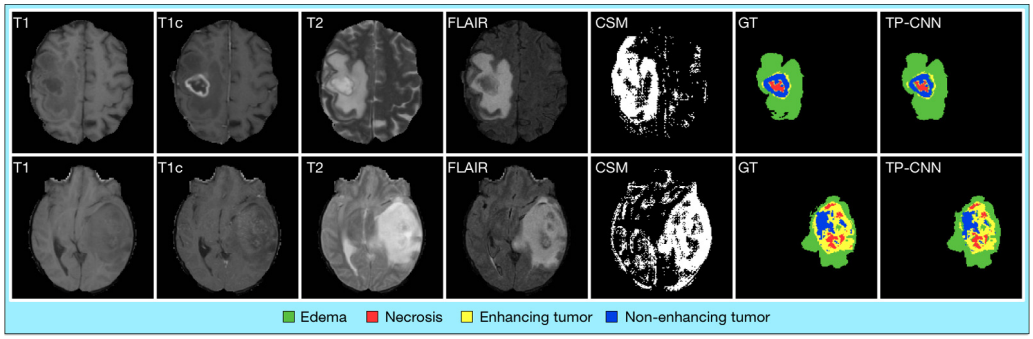


**Fig. 8.** Presents the proposed TP-CNN method's results for HGG and LGG MRI modalities. First row shows the result for HGG patient whereas the second row presents the result for LGG patient. The T1, T1c, T2 and FLAIR are MRI modalities, CSM stands for SVM predicted CSM, GT presents the provided ground truth. TP-CNN presents our proposed method's segmentation of brain tumor. The figure is best viewed in color. (For interpretation of the references to color in this figure legend, the reader is referred to the web version of this article.)

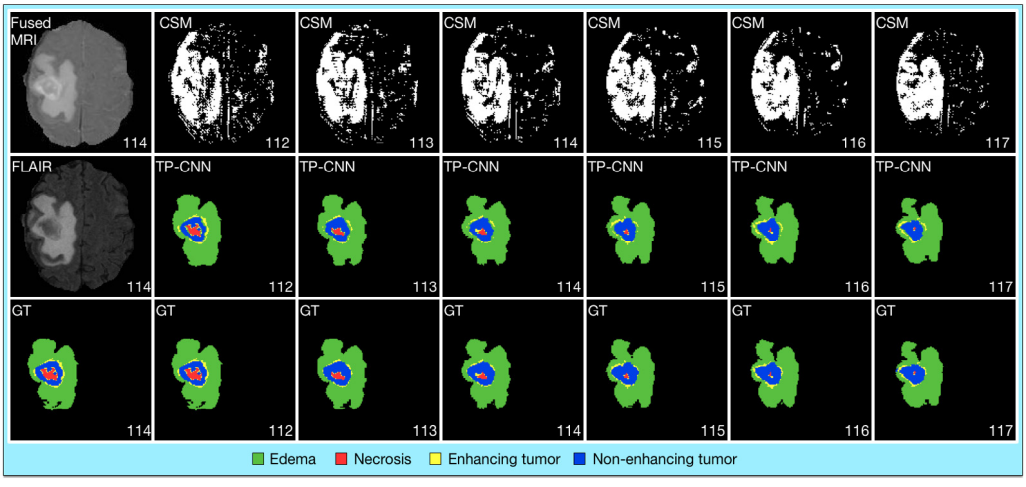


**Fig. 9.** Presents the proposed TP-CNN method's slice wise results for HGG MRI. First row shows the slice wise generated CSM using trained SVM. The number in the bottom right corner presents the corresponding slice number. Second row shows the slice wise results of our prosposed HGG TP-CNN method. Third row shows respective ground truth slices with slice number in bottom right corner. GT presents provided ground truth. The figure is best viewed in color. (For interpretation of the references to color in this figure legend, the reader is referred to the web version of this article.)

## 6. Conclusion

In this paper, a cascaded approach for fully automatic brain tumor segmentation using IoT generated images has been presented, which intelligently combines handcrafted features-based technique and CNN. Three handcrafted features are extracted in a spatial neighborhood of size 7 × 7 which were passed to SVM resulting in CSM which served as the prior knowledge and was fed to novel three pathways

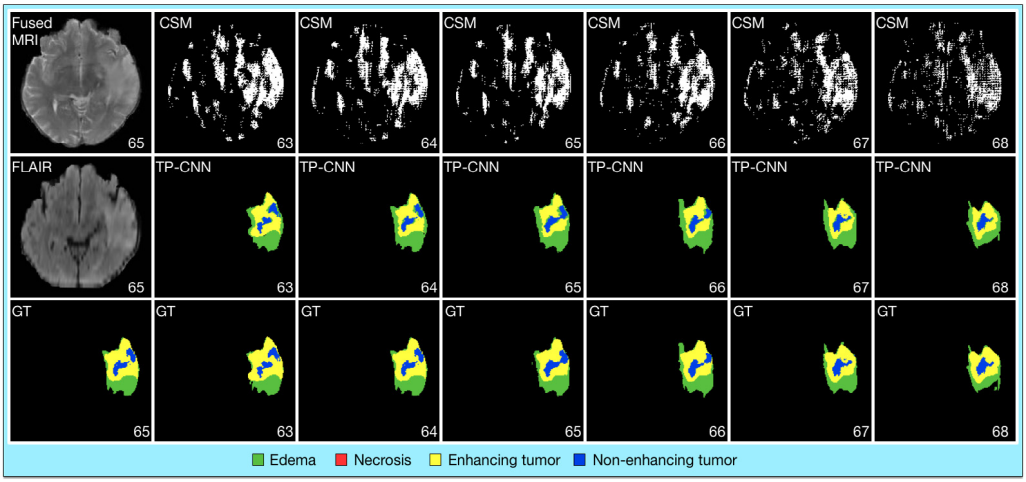


**Fig. 10.** Presents the proposed TP-CNN method's slice-wise results for LGG MRI. First row shows the slice-wise generated CSM using trained SVM. The number in the bottom right corner presents the corresponding slice number. Second row shows the slice-wise results of LGG TP-CNN. Third row shows the respective ground truth slices with slice number in bottom right corner. GT shows provided ground truth. The figure is best viewed in color. (For interpretation of the references to color in this figure legend, the reader is referred to the web version of this article.)

**Table 3**
Results of our proposed method for individual HGG and LGG TP-CNN in terms of mean DSS and standard deviation.

| Method | Complete | Core | Enhancing |
|---|---|---|---|
| HGG | 0.83 ± 0.035 | 0.78 ± 0.095 | 0.74 ± 0.083 |
| LGG | 0.79 ± 0.073 | 0.74 ± 0.120 | 0.72 ± 0.088 |
| Mean | 0.81 ± 0.054 | 0.76 ± 0.107 | 0.73 ± 0.085 |

**Table 4**
Performance evaluation using BRATS-2015 dataset and comparison with 2D-CNN and other ML state-of-art methods.

| Method | Complete | Core | Enhancing |
|---|---|---|---|
| **TP-CNN** | **0.81** | **0.76** | **0.73** |
| Peraira et al. [33] | 0.78 | 0.65 | 0.75 |
| Agn et al. [45] | 0.77 | 0.64 | 0.52 |
| Kuanlun et al. [81] | 0.75 | 0.77 | 0.76 |
| Zhao et al. [82] | 0.80 | 0.68 | 0.65 |
| Song et al. [83] | 0.852 | 0.70 | 0.734 |
| Randhawa et al. [84] | 0.87 | 0.75 | 0.71 |

CNN architecture along with the given MRIs. Our experiments on BRATS 2015 dataset showed promising results (especially on outer tumor boundaries, i.e. edema). In the future, a separate prior will be provided on each tumor type (i.e. necrosis, non-enhancing, enhancing and edema) which is likely to increase the segmentation accuracy of sub-tumor types.

## Declaration of competing interest

The authors declare that they have no known competing financial interests or personal relationships that could have appeared to influence the work reported in this paper.

## CRediT authorship contribution statement

**Hikmat Khan:** Conceptualization, Methodology, Writing - original draft. **Pir Masoom Shah:** Conceptualization, Methodology, Writing - original draft. **Munam Ali Shah:** Supervision, Conceptualization, Validation. **Saif ul Islam:** Writing - review & editing. **Joel J.P.C. Rodrigues:** Funding acquisition, Methodology, Validation, Writing - review & editing.

## Acknowledgments

This work was partially supported by FCT/MCTES, Portugal through national funds and when applicable co-funded EU funds under the project UIDB/EEA/50008/2020; and by the Brazilian National Council for Scientific and Technological Development (CNPq) via Grant No. 309335/
2017-5.

## References

[1] A.F. Santamaria, F. De Rango, A. Serianni, P. Raimondo, A real IoT device deployment for e-health applications under lightweight communication protocols, activity classifier and edge data filtering, Comput. Commun. 128 (2018) 60–73.
[2] F. Ali, S.R. Islam, D. Kwak, P. Khan, N. Ullah, S.-j. Yoo, K.S. Kwak, Type-2 fuzzy ontology–aided recommendation systems for IoT–based healthcare, Comput. Commun. 119 (2018) 138–155.
[3] L.Y. Mano, B.S. Faiçal, L.H. Nakamura, P.H. Gomes, G.L. Libralon, R.I. Meneguete, P. Geraldo Filho, G.T. Giancristofaro, G. Pessin, B. Krishnamachari, et al., Exploiting IoT technologies for enhancing health smart homes through patient identification and emotion recognition, Comput. Commun. 89 (2016) 178–190.
[4] A. Caragliu, C. Del Bo, P. Nijkamp, Smart cities in Europe, J. Urban Technol. 18 (2) (2011) 65–82.
[5] I.U. Din, M. Guizani, J.J. Rodrigues, S. Hassan, V.V. Korotaev, Machine learning in the Internet of Things: Designed techniques for smart cities, Future Gener. Comput. Syst. 100 (2019) 826–843.
[6] M.U. Younus, S. ul Islam, I. Ali, S. Khan, M.K. Khan, A survey on software defined networking enabled smart buildings: Architecture, challenges and use cases, J. Netw. Comput. Appl. 137 (2019) 62–77.
[7] F. Bhatti, M.A. Shah, C. Maple, S.U. Islam, A novel Internet of Things-enabled accident detection and reporting system for smart city environments, Sensors 19 (9) (2019) 2071.
[8] P.H. Vilela, J.J. Rodrigues, P. Solic, K. Saleem, V. Furtado, Performance evaluation of a fog-assisted IoT solution for e-health applications, Future Gener. Comput. Syst. 97 (2019) 379–386.
[9] O. Betul, M. Ipek, Brain tumor presenting with psychiatric symptoms, J. Neuropsychiatry Clinic. Neurosci. 23 (4) (2011) E43–E44.
[10] P. Rajan, C. Sundar, Brain tumor detection and segmentation by intensity adjustment, J. Med. Syst. 43 (8) (2019) 282.
[11] Quick brain tumor facts, 2009, http://braintumor.org/brain-tumor-information/brain-tumor-facts/. (Accessed 2017-05-09).
[12] D.N. Louis, H. Ohgaki, O.D. Wiestler, W.K. Cavenee, P.C. Burger, A. Jouvet, B.W. Scheithauer, P. Kleihues, The 2007 WHO classification of tumours of the central nervous system, Acta Neuropathol. 114 (2) (2007) 97–109.
[13] B.H. Menze, A. Jakab, S. Bauer, J. Kalpathy-Cramer, K. Farahani, J. Kirby, Y. Burren, N. Porz, J. Slotboom, R. Wiest, et al., The multimodal brain tumor image segmentation benchmark (BRATS), IEEE Trans. Med. Imaging 34 (10) (2015) 1993–2024.

[14] N.J. Tustison, B.B. Avants, P.A. Cook, Y. Yuanjie Zheng, A. Egan, P.A. Yushkevich, J.C. Gee, N4ITK: Improved N3 bias correction, IEEE Trans. Med. Imaging 29 (6) (2010) 1310–1320.
[15] L. Nyul, J. Udupa, X. Xuan Zhang, New variants of a method of MRI scale standardization, IEEE Trans. Med. Imaging 19 (2) (2000) 143–150.
[16] B. Menze, A. Jakab, M. Reyes, Prastawa, MICCAI 2013 challenge on multimodal brain tumor segmentation, in: Proceedings of the MICCAI-BRATS, IEEE, Nagoya, Japan, 2013, URL http://martinos.org/qtim/miccai2013/.
[17] B. Menze, A. Jakab, M. Reyes, Prastawa, MICCAI 2014 challenge on multimodal brain tumor segmentation, in: Proceedings of the MICCAI-BRATS, IEEE, Boston, Massachusetts, 2014, URL https://sites.google.com/site/miccaibrats2014/.
[18] B.H. Menze, A. Jakab, S. Bauer, J. Kalpathy-Cramer, K. Farahani, J. Kirby, Y. Burren, N. Porz, J. Slotboom, R. Wiest, et al., The multimodal brain tumor image segmentation benchmark (BRATS), IEEE Trans. Med. Imaging 34 (10) (2015) 1993–2024.
[19] R. Meier, S. Bauer, J. Slotboom, R. Wiest, M. Reyes, A hybrid model for multimodal brain tumor segmentation, Multimodal Brain Tumor Segm. 31 (2013).
[20] R. Meier, S. Bauer, J. Slotboom, R. Wiest, M. Reyes, Appearance-and context-sensitive features for brain tumor segmentation, in: Proceedings of MICCAI BRATS Challenge, pp. 020–026.
[21] N.J. Tustison, K. Shrinidhi, M. Wintermark, C.R. Durst, B.M. Kandel, J.C. Gee, M.C. Grossman, B.B. Avants, Optimal symmetric multimodal templates and concatenated random forests for supervised brain tumor segmentation (simplified) with ANTsR, Neuroinformatics 13 (2) (2015) 209–225.
[22] N. Dalal, B. Triggs, Histograms of oriented gradients for human detection, in: Computer Vision and Pattern Recognition, 2005. CVPR 2005. IEEE Computer Society Conference on, vol. 1, IEEE, 2005, pp. 886–893.
[23] T. Ahonen, A. Hadid, M. Pietikainen, Face description with local binary patterns: Application to face recognition, IEEE Trans. Pattern Anal. Mach. Intell. 28 (12) (2006) 2037–2041.
[24] P. Georgiadis, D. Cavouras, I. Kalatzis, A. Daskalakis, G.C. Kagadis, K. Sifaki, M. Malamas, G. Nikiforidis, E. Solomou, Improving brain tumor characterization on MRI by probabilistic neural networks and non-linear transformation of textural features, Comput. Methods Programs Biomed. 89 (1) (2008) 24–32.
[25] S. Bauer, L.-P. Nolte, M. Reyes, Fully automatic segmentation of brain tumor images using support vector machine classification in combination with hierarchical conditional random field regularization, in: International Conference on Medical Image Computing and Computer-Assisted Intervention, Springer, 2011, pp. 354–361.
[26] M. Havaei, H. Larochelle, P. Poulin, P.-M. Jodoin, Within-brain classification for brain tumor segmentation, Int. J. Comput. Assist. Radiol. Surg. 11 (5) (2016) 777–788.
[27] A. Islam, S.M. Reza, K.M. Iftekharuddin, Multifractal texture estimation for detection and segmentation of brain tumors, IEEE Trans. Biomed. Eng. 60 (11) (2013) 3204–3215.
[28] D. Zikic, B. Glocker, E. Konukoglu, A. Criminisi, C. Demiralp, J. Shotton, O. Thomas, T. Das, R. Jena, S. Price, Decision forests for tissue-specific segmentation of high-grade gliomas in multi-channel MR, in: Medical Image Computing and Computer-Assisted Intervention–MICCAI 2012, Springer, 2012, pp. 369–376.
[29] B. Menze, A. Jakab, S. Bauer, The multimodal brain tumor image segmentation benchmark (BRATS), IEEE Trans. Med. Imaging 34 (10) (2014) 1993–2024, http://dx.doi.org/10.1109/TMI.2014.2377694, URL https://hal.inria.fr/hal-00935640.
[30] G. Urban, M. Bendszus, F. Hamprecht, J. Kleesiek, Multi-modal brain tumor segmentation using deep convolutional neural networks, MICCAI (BRATS) (Brain Tumor Segmentation) Challenge. Proceedings, Winning Contribution, 2014, pp. 31–35.
[31] O. Yi, D. and Zhou, M. and Chen, Z. and Gevaert, 3-D Convolutional neural networks for glioblastoma segmentation, 2016, arXiv preprint arXiv:1611.04534 [cs.CV].
[32] D. Zikic, Y. Ioannou, M. Brown, A. Criminisi, Segmentation of brain tumor tissues with convolutional neural networks, in: Proceedings of MICCAI-BRATS, 2014, pp. 36–39.
[33] C. Pereira, S., Pinto, A., Alves, V. and Silva, Brain tumor segmentation using convolutional neural networks in MRI images, IEEE Trans. Med. Imaging 35 (5) (2016) 1240–1251.
[34] M. Havaei, A. Davy, D. Warde-Farley, A. Biard, A. Courville, Y. Bengio, C. Pal, P.-M. Jodoin, H. Larochelle, Brain tumor segmentation with deep neural networks, Med. Image Anal. 35 (2017) 18–31.
[35] M. Cabezas, A. Oliver, X. Lladó, J. Freixenet, M.B. Cuadra, A review of atlas-based segmentation for magnetic resonance brain images, Comput. Methods Programs Biomed. 104 (3) (2011) e158–e177.
[36] J. Jiang, Y. Wu, M. Huang, W. Yang, W. Chen, Q. Feng, 3D brain tumor segmentation in multimodal MR images based on learning population-and patient-specific feature sets, Comput. Med. Imaging Graph. 37 (7) (2013) 512–521.
[37] B.N. Saha, N. Ray, R. Greiner, A. Murtha, H. Zhang, Quick detection of brain tumors and edemas: A bounding box method using symmetry, Comput. Med. Imaging Graph. 36 (2) (2012) 95–107.
[38] K. Thapaliya, J.-Y. Pyun, C.-S. Park, G.-R. Kwon, Level set method with automatic selective local statistics for brain tumor segmentation in MR images, Comput. Med. Imaging Graph. 37 (7) (2013) 522–537.
[39] M. Prastawa, E. Bullitt, S. Ho, G. Gerig, A brain tumor segmentation framework based on outlier detection, Med. Image Anal. 8 (3) (2004) 275–283.
[40] S. Iqbal, M.U. Ghani, T. Saba, A. Rehman, Brain tumor segmentation in multi-spectral MRI using convolutional neural networks (CNN), Microsc. Res. Tech. 81 (4) (2018) 419–427, http://dx.doi.org/10.1002/jemt.22994, URL https://app.dimensions.ai/details/publication/pub.1100553678.
[41] S. Nema, A. Dudhane, S. Murala, S. Naidu, RescueNet: An unpaired GAN for brain tumor segmentation, Biomed. Signal Process. Control 55 (2020) 101641, http://dx.doi.org/10.1016/j.bspc.2019.101641, URL http://www.sciencedirect.com/science/article/pii/S1746809419302228.
[42] M. Sajjad, S. Khan, K. Muhammad, W. Wu, A. Ullah, S.W. Baik, Multi-grade brain tumor classification using deep CNN with extensive data augmentation, J. Comput. Sci. 30 (2019) 174–182, http://dx.doi.org/10.1016/j.jocs.2018.12.003, URL http://www.sciencedirect.com/science/article/pii/S1877750318307385.
[43] M. Schmidt, I. Levner, R. Greiner, A. Murtha, A. Bistritz, Segmenting brain tumors using alignment-based features, in: Machine Learning and Applications, 2005. Proceedings. Fourth International Conference on, IEEE, 2005, pp. 6–pp.
[44] D.T. Gering, W. Grimson, R. Kikinis, Recognizing deviations from normalcy for brain tumor segmentation, in: International Conference on Medical Image Computing and Computer-Assisted Intervention, Springer, 2002, pp. 388–395.
[45] M. Agn, O. Puonti, P.M. af Rosenschöld, I. Law, K. Van Leemput, Brain tumor segmentation using a generative model with an RBM prior on tumor shape, in: International Workshop on Brainlesion: Glioma, Multiple Sclerosis, Stroke and Traumatic Brain Injuries, Springer, 2015, pp. 168–180.
[46] A. Hamamci, N. Kucuk, K. Karaman, K. Engin, G. Unal, Tumor-cut: segmentation of brain tumors on contrast enhanced MR images for radiosurgery applications, IEEE Trans. Med. Imaging 31 (3) (2012) 790–804.
[47] H. Khotanlou, O. Colliot, J. Atif, I. Bloch, 3D brain tumor segmentation in MRI using fuzzy classification, symmetry analysis and spatially constrained deformable models, Fuzzy Sets and Systems 160 (10) (2009) 1457–1473.
[48] N.K. Subbanna, D. Precup, D.L. Collins, T. Arbel, Hierarchical probabilistic Gabor and MRF segmentation of brain tumours in MRI volumes, in: International Conference on Medical Image Computing and Computer-Assisted Intervention, Springer, 2013, pp. 751–758.
[49] O.S. Al-Kadi, A multiresolution clinical decision support system based on fractal model design for classification of histological brain tumours, Comput. Med. Imaging Graph. 41 (2015) 67–79.
[50] S. Bauer, R. Wiest, L.-P. Nolte, M. Reyes, A survey of MRI-based medical image analysis for brain tumor studies, Phys. Med. Biol. 58 (13) (2013) R97.
[51] E.I. Zacharaki, S. Wang, S. Chawla, D. Soo Yoo, R. Wolf, E.R. Melhem, C. Davatzikos, Classification of brain tumor type and grade using MRI texture and shape in a machine learning scheme, Magn. Reson. Med. 62 (6) (2009) 1609–1618.
[52] N. Subbanna, D. Precup, T. Arbel, Iterative multilevel MRF leveraging context and voxel information for brain tumour segmentation in MRI, in: Proceedings of the IEEE Conference on Computer Vision and Pattern Recognition, 2014, pp. 400–405.
[53] K.K. Reddy, B. Solmaz, P. Yan, N.G. Avgeropoulos, D.J. Rippe, M. Shah, Confidence guided enhancing brain tumor segmentation in multi-parametric MRI, in: Biomedical Imaging, ISBI, 2012 9th IEEE International Symposium on, IEEE, 2012, pp. 366–369.
[54] G. Wang, W. Li, M. Aertsen, J. Deprest, S. Ourselin, T. Vercauteren, Aleatoric uncertainty estimation with test-time augmentation for medical image segmentation with convolutional neural networks, Neurocomputing 338 (2019) 34–45.
[55] S. Srinivas, R.K. Sarvadevabhatla, K.R. Mopuri, N. Prabhu, S.S. Kruthiventi, R.V. Babu, A taxonomy of deep convolutional neural nets for computer vision, 2016, arXiv preprint arXiv:1601.06615.
[56] A. Krizhevsky, I. Sutskever, G.E. Hinton, Imagenet classification with deep convolutional neural networks, in: Advances in Neural Information Processing Systems, 2012, pp. 1097–1105.
[57] P. Sudharshan, C. Petitjean, F. Spanhol, L.E. Oliveira, L. Heutte, P. Honeine, Multiple instance learning for histopathological breast cancer image classification, Expert Syst. Appl. 117 (2019) 103–111.
[58] D. Han, Q. Liu, W. Fan, A new image classification method using CNN transfer learning and web data augmentation, Expert Syst. Appl. 95 (2018) 43–56.
[59] S.J. Shri, S. Jothilakshmi, Crowd video event classification using convolutional neural network, Comput. Commun. 147 (2019) 35–39.
[60] K. Jarrett, K. Kavukcuoglu, Y. LeCun, et al., What is the best multi-stage architecture for object recognition? in: Computer Vision, 2009 IEEE 12th International Conference on, IEEE, 2009, pp. 2146–2153.
[61] Z.-Y. Shen, S.-Y. Han, L.-C. Fu, P.-Y. Hsiao, Y.-C. Lau, S.-J. Chang, Deep convolution neural network with scene-centric and object-centric information for object detection, Image Vis. Comput. 85 (2019) 14–25.
[62] V. Bhanumathi, R. Sangeetha, CNN based training and classification of MRI brain images, in: 2019 5th International Conference on Advanced Computing & Communication Systems, ICACCS, IEEE, 2019, pp. 129–133.
[63] B. Kayalibay, G. Jensen, P. van der Smagt, CNN-based segmentation of medical imaging data, 2017, arXiv preprint arXiv:1701.03056.

[64] S. Hussain, S.M. Anwar, M. Majid, Segmentation of glioma tumors in brain using deep convolutional neural network, Neurocomputing 282 (2018) 248–261.
[65] K. Simonyan, A. Zisserman, Very deep convolutional networks for large-scale image recognition, 2014, arXiv preprint arXiv:1409.1556.
[66] M. Havaei, A. Davy, D. Warde-Farley, A. Biard, A. Courville, Y. Bengio, C. Pal, P.-M. Jodoin, H. Larochelle, Brain tumor segmentation with deep neural networks, Med. Image Anal. 35 (2017) 18–31.
[67] M. Pietikäinen, T. Ojala, Z. Xu, Rotation-invariant texture classification using feature distributions, Pattern Recognit. 33 (1) (2000) 43–52.
[68] L. Liu, L. Zhao, Y. Long, G. Kuang, P. Fieguth, Extended local binary patterns for texture classification, Image Vis. Comput. 30 (2) (2012) 86–99.
[69] Brain tumor statistics | abta.org, 2009, http://www.abta.org/about-us/news/brain-tumor-statistics/. (Accessed 2017-05-09).
[70] C.J. Burges, A tutorial on support vector machines for pattern recognition, Data Min. Knowl. Discov. 2 (2) (1998) 121–167.
[71] R. Giryes, G. Sapiro, A.M. Bronstein, Deep neural networks with random gaussian weights: A universal classification strategy, CoRR abs/1504.08291 (2015).
[72] X. Glorot, Y. Bengio, Understanding the difficulty of training deep feedforward neural networks., in: Aistats, Vol. 9, 2010, pp. 249–256.
[73] A.L. Maas, A.Y. Hannun, A.Y. Ng, Rectifier nonlinearities improve neural network acoustic models, in: Proc. ICML, 2013.
[74] Y. LeCun, Y. Bengio, G. Hinton, Deep learning, Nature 521 (7553) (2015) 436–444.
[75] N. Srivastava, G.E. Hinton, A. Krizhevsky, I. Sutskever, R. Salakhutdinov, Dropout: a simple way to prevent neural networks from overfitting., J. Mach. Learn. Res. 15 (1) (2014) 1929–1958.
[76] C.M. Bishop, Pattern recognition, Mach. Learn. 128 (2006) 1–736.
[77] R.C. Gonzalez, R.E. Woods, Digital Image Processing, third ed., Prentice-Hall, Inc., Upper Saddle River, NJ, USA, 2006.
[78] Scikit-learn:machine learning in python, 2009, http://scikit-learn.org/stable/. (Accessed 2017-05-09).
[79] Keras: deep learning library for theano and tensorflow, 2009, https://keras.io/. (Accessed 2017-05-09).
[80] Simplified insight segmentation and registration toolkit (SimpleITK), 2009, http://www.simpleitk.org/. (Accessed 2017-05-09).
[81] T. Lun, W. Hsu, Brain tumor segmentation using deep convolutional neural network, in: Proceedings of BRATS-MICCAI, 2016.
[82] X. Zhao, Y. Wu, G. Song, Z. Li, Y. Fan, Y. Zhang, Brain tumor segmentation using a fully convolutional neural network with conditional random fields, in: International Workshop on Brainlesion: Glioma, Multiple Sclerosis, Stroke and Traumatic Brain Injuries, Springer, 2016, pp. 75–87.
[83] B. Song, C.-R. Chou, X. Chen, A. Huang, M.-C. Liu, Anatomy-guided brain tumor segmentation and classification, in: International Workshop on Brainlesion: Glioma, Multiple Sclerosis, Stroke and Traumatic Brain Injuries, Springer, 2016, pp. 162–170.
[84] R. Randhawa, A. Modi, P. Jain, P. Warier, Improving segment boundary classification for Brain Tumor Segmentation and longitudinal disease progression, in: BrainLes 2016, 2016, pp. 65–74.